

Linear Perturbations and Multi-Probe Diagnostics in Dark-Sector Selective $f(R, T_\chi)$ Gravity

L. Yıldız^{*1}, D. Kayki^{†2}, and E. Güdekli^{‡3}

^{1,2,3}Department of Physics, Faculty of Science, Istanbul University,
Istanbul 34134, Turkey

Abstract

We develop a dark-sector selective trace-coupled extension of gravity in which the matter–curvature coupling depends exclusively on the trace of the dark-matter energy–momentum tensor, T_χ , defined from a canonical dark-matter field χ . This construction provides a microphysically specified trace sector, removes the usual matter-Lagrangian ambiguity of $f(R, T)$ -type models, and preserves minimal coupling of visible matter by design. We derive the full field equations, the exact dark-sector exchange structure, and the linear scalar-perturbation system in gauge-ready form. In the sub-horizon regime, we derive effective modified-gravity functions governing structure growth and light deflection, and show that the model generically produces correlated, scale- and time-dependent departures from General Relativity in growth and lensing observables. Building on this structure, we formulate a perturbation-focused multi-probe framework based on redshift-space distortions, weak lensing, and CMB lensing, explicitly targeting degeneracy breaking beyond background-expansion tests. The analysis establishes the action-level and perturbation-level foundations of the model and provides a conservative, reproducible framework for translated linear-regime constraints within a dark-sector selective modified-gravity setting.

Keywords: dark sector, $f(R, T)$ gravity, trace coupling, cosmological perturbations, structure growth, gravitational lensing

Highlights

- Dark-sector-only T_χ coupling removes direct visible-matter trace coupling at the action level

^{*}li.yildiz.na@gmail.com

[†]deha.kayki@ogr.iu.edu.tr

[‡]gudekli@istanbul.edu.tr

- Microphysical canonical- χ construction removes the L_m ambiguity of $f(R, T)$ -type models
- Linear scalar perturbations yield scale- and time-dependent growth and lensing signatures
- Perturbation-level multi-probe diagnostics target background-only degeneracies in modified gravity

1 Introduction

The physical nature of the dark sector remains one of the most persistent open problems in fundamental physics and cosmology [2, 5]. The concordance Λ CDM framework provides an excellent effective description of a broad range of observations[1], yet it leaves the microphysics of dark matter and dark energy unspecified [2, 5]. This motivates theoretically controlled extensions that are both internally consistent and empirically testable [4, 5]. In particular, many beyond- Λ CDM scenarios are nearly degenerate at the level of background expansion, so their viability must be assessed primarily through *perturbation-sensitive* signatures such as the growth of cosmic structure and the deflection of light [3, 4, 29]. A modified-gravity framework aimed at the dark sector should therefore deliver predictive, falsifiable correlations between growth and lensing observables rather than relying on background fits alone [4, 5].

Trace-coupled modifications of gravity provide a phenomenologically rich arena to explore such signatures [6, 8]. In the standard $f(R, T)$ class, the gravitational Lagrangian depends on the Ricci scalar R and the trace of the matter stress-energy tensor T , enabling an effective interaction between matter and geometry [6]. However, two recurrent issues arise in generic $f(R, T)$ constructions [6, 7]. First, the theory can inherit an ambiguity associated with the choice of the matter Lagrangian density L_m and the related tensor $\Theta_{\mu\nu}$, which affects the precise form of the field equations and the exchange terms. Second, if visible matter couples directly to the modified sector, baryonic fifth-force constraints and local tests of gravity can severely restrict the parameter space [9, 8]. These issues become particularly acute when one attempts to build a predictive perturbation theory suitable for confrontation with large-scale-structure and lensing measurements [4, 8].

In this work we address both problems by introducing a *dark-sector selective* trace coupling in which the modified-gravity dependence on the matter trace is restricted to the *dark-matter* sector only, $T \rightarrow T_\chi$. Visible matter components (baryons and radiation) remain minimally coupled by construction, suppressing direct baryonic fifth-force effects at the level of the fundamental action. In addition, we define the dark matter microphysically by a canonical field χ , so that T_χ and $\Theta_{\mu\nu}^{(\chi)}$ are uniquely determined. This choice removes the standard L_m ambiguity and yields an unambiguous exchange structure between the dark sector and the modified gravitational dynamics.

The construction is intended as a minimal, physically interpretable, and observationally testable effective framework, rather than a unique UV-complete theory. Its purpose is to isolate curvature–dark-sector coupling effects in the sector where late-time cosmological degeneracies are most likely to appear, while preserving a clean separation from visible-sector dynamics at the level of the fundamental action. This separation does not imply that visible-sector observables are unaffected; rather, their response is mediated indirectly through the modified gravitational dynamics, not through a direct trace coupling in the matter action. In this sense, the model provides a controlled setting in which the impact of selective trace coupling can be tracked consistently from background evolution to linear perturbations and, ultimately, to multi-probe observables.

Our primary goal is to develop a perturbation-complete and observationally relevant framework for this class of models. We derive the full field equations and the exact dark-sector exchange relations implied by the selective coupling, and we obtain the linear scalar perturbation system in a gauge-ready form suitable for direct implementation in numerical pipelines. In the sub-horizon regime, we show how the theory can be mapped to effective modified-gravity functions that control the clustering of matter and the deflection of light, enabling predictions for redshift-space distortions (via $f\sigma_8$) and for weak and CMB lensing [16, 4, 8]. This multi-probe focus is essential to break background-level degeneracies and to isolate signatures that distinguish the model from General Relativity and Λ CDM [3, 4, 5].

Positioning relative to other modified-gravity frameworks. The construction is intended to occupy an intermediate position between fully generic trace-coupled models and purely phenomenological late-time parameterizations. Compared with generic $f(R, T)$ theories, the restriction $T \rightarrow T_\chi$ and the microphysical canonical-scalar realization of the dark sector remove the usual matter-Lagrangian ambiguity and prevent direct trace coupling to visible matter at the level of the fundamental action, while retaining a non-trivial matter–curvature exchange structure in the dark sector [6]. Compared with pure $f(R)$ models, the selective RT_χ and T_χ^2 channels enlarge the perturbation-level phenomenology by introducing an explicit dark-sector trace response in addition to the standard curvature (scalaron) sector [10]. Finally, unlike model-independent effective descriptions that parameterize modified growth and lensing directly at the level of linear perturbations (e.g. EFT/Horndeski-inspired or (μ, Σ) -type approaches), the framework retains an explicit action-level parametrization with a transparent map from Lagrangian coefficients (α, ξ, β) to background and perturbation quantities, which is useful for implementation-ready and falsifiable multi-probe inference analyses [11, 12, 13].

From the viewpoint of local-gravity phenomenology, the selective restriction $T \rightarrow T_\chi$ is also advantageous: because visible matter remains minimally coupled in the matter action, the model avoids direct baryonic trace-coupling effects at the fundamental level. This does not eliminate the need for screening or local-gravity consistency tests, since visible-sector observables can still be af-

affected indirectly through the modified gravitational dynamics, but it provides a cleaner starting point than generic trace-coupled constructions for incorporating environment-dependent screening mechanisms.

The paper is organized as follows. In Sec. 2 we introduce the dark-sector selective $f(R, T_\chi)$ action, define the microphysical dark-matter sector, and derive the field equations together with their conservation and exchange structure. In Sec. 3 we specialize the theory to an FLRW background and obtain the modified cosmological evolution equations. In Sec. 4 we derive the linear perturbation equations and identify the effective functions governing growth and lensing. In Sec. 5 we connect the theoretical predictions to perturbation-sensitive observables and outline a multi-probe inference strategy. We conclude in Sec. 8 with a summary and outlook.

2 Dark-sector selective $f(R, T_\chi)$ framework

2.1 Conventions and definitions

We adopt metric signature $(-, +, +, +)$ and units $c = \hbar = 1$. The covariant derivative is ∇_μ and $\square \equiv g^{\mu\nu} \nabla_\mu \nabla_\nu$. We define the partial derivatives of the gravitational function as

$$f_R \equiv \frac{\partial f}{\partial R}, \quad f_T \equiv \frac{\partial f}{\partial T_\chi}. \quad (1)$$

2.2 Action and matter content

We consider a trace-coupled extension in which the *gravitational trace dependence* is restricted to the dark-matter trace T_χ , while visible components remain minimally coupled. The action is

$$S = \int d^4x \sqrt{-g} \left[\frac{1}{2\kappa^2} f(R, T_\chi) + \mathcal{L}_b + \mathcal{L}_{\text{rad}} + \mathcal{L}_\chi \right], \quad (2)$$

where $\kappa^2 \equiv 8\pi G$ and \mathcal{L}_b and \mathcal{L}_{rad} denote baryons and radiation.

This construction is adopted as a dark-sector selective extension of the $f(R, T)$ framework [6], in which the trace dependence of the gravitational sector is restricted to T_χ rather than the total matter trace. The motivation is twofold: it preserves a clean phenomenological separation between visible-sector dynamics and dark-sector backreaction channels, and it isolates the modified coupling to the sector where late-time cosmological degeneracies and beyond- Λ CDM signatures are most naturally probed in a controlled way. In this sense, the model is treated throughout as a minimal, physically interpretable, and observationally testable effective framework, rather than a unique UV-complete theory.

To remove the usual matter-Lagrangian ambiguity present in generic $f(R, T)$ scenarios, we define dark matter microphysically as a canonical scalar field χ ,

$$\mathcal{L}_\chi = -\frac{1}{2} g^{\mu\nu} \partial_\mu \chi \partial_\nu \chi - V(\chi). \quad (3)$$

The corresponding stress-energy tensor follows from $T_{\mu\nu}^{(\chi)} \equiv -\frac{2}{\sqrt{-g}} \frac{\delta(\sqrt{-g}\mathcal{L}_\chi)}{\delta g^{\mu\nu}}$, giving

$$T_{\mu\nu}^{(\chi)} = \partial_\mu\chi \partial_\nu\chi - g_{\mu\nu} \left[\frac{1}{2}(\partial\chi)^2 + V(\chi) \right], \quad (4)$$

with $(\partial\chi)^2 \equiv g^{\rho\sigma} \partial_\rho\chi \partial_\sigma\chi$. Its trace is

$$T_\chi \equiv g^{\mu\nu} T_{\mu\nu}^{(\chi)} = -(\partial\chi)^2 - 4V(\chi). \quad (5)$$

With the canonical choice (3), both T_χ and the metric variation entering $\Theta_{\mu\nu}^{(\chi)}$ are fixed uniquely, so the f_T -induced exchange terms are defined without the matter-Lagrangian ambiguity that affects generic phenomenological $f(R, T)$ implementations [6, 7].

The restriction $T \rightarrow T_\chi$ in Eq. (2) defines a *dark-sector selective* matter-curvature coupling. Visible matter is assumed to be minimally coupled through \mathcal{L}_b and \mathcal{L}_{rad} , so that standard local constraints associated with direct baryonic couplings are avoided at the level of the fundamental action [9, 8]. This does not imply that visible-sector observables are unaffected; rather, their response is mediated indirectly through the modified gravitational dynamics, not through a direct trace coupling in the matter action. In the next subsection we derive the modified field equations and the exact exchange structure induced by $f_T \neq 0$, which will be the basis for the background and linear perturbation analysis.

2.3 Field equations and dark-sector exchange structure

Varying the action (2) with respect to the metric yields the modified field equations. Writing $f_R \equiv \partial f / \partial R$ and $f_T \equiv \partial f / \partial T_\chi$, one obtains

$$f_R R_{\mu\nu} - \frac{1}{2} f g_{\mu\nu} + (g_{\mu\nu} \square - \nabla_\mu \nabla_\nu) f_R = \kappa^2 \left(T_{\mu\nu}^{(b)} + T_{\mu\nu}^{(\text{rad})} + T_{\mu\nu}^{(\chi)} \right) - f_T \left(T_{\mu\nu}^{(\chi)} + \Theta_{\mu\nu}^{(\chi)} \right), \quad (6)$$

where the tensor $\Theta_{\mu\nu}^{(\chi)}$ is defined by

$$\Theta_{\mu\nu}^{(\chi)} \equiv g^{\alpha\beta} \frac{\delta T_{\alpha\beta}^{(\chi)}}{\delta g^{\mu\nu}}. \quad (7)$$

Because the trace coupling is restricted to T_χ , only the dark-matter sector enters the f_T term; visible matter remains minimally coupled.

Closed form of $\Theta_{\mu\nu}^{(\chi)}$ for canonical χ

For the canonical scalar field defined in Eq. (3), $\Theta_{\mu\nu}^{(\chi)}$ is uniquely determined. Using the standard identity for minimally coupled matter, one finds the closed form [6, 7]

$$\Theta_{\mu\nu}^{(\chi)} = -2T_{\mu\nu}^{(\chi)} + g_{\mu\nu} \mathcal{L}_\chi = g_{\mu\nu} \left[\frac{1}{2}(\partial\chi)^2 + V(\chi) \right] - 2\partial_\mu\chi \partial_\nu\chi. \quad (8)$$

A particularly useful simplification is

$$T_{\mu\nu}^{(\chi)} + \Theta_{\mu\nu}^{(\chi)} = -\partial_\mu\chi\partial_\nu\chi, \quad (9)$$

which makes the structure of the trace coupling especially transparent.

The canonical scalar-field description (3) is adopted as a minimal microphysical realisation of the dark sector that fixes T_χ and the metric variation entering $\Theta_{\mu\nu}^{(\chi)}$ unambiguously, thereby enabling a perturbation-complete and implementation-ready formulation of the theory. We do not interpret χ as a unique fundamental particle-physics model of dark matter; rather, it serves as a representative low-energy effective degree of freedom capturing a broad class of scalar dark-matter scenarios (e.g. ultralight/axion-like fields or moduli in cosmology) at the level relevant for background and linear-perturbation dynamics [17, 18, 19]. The framework can be straightforwardly generalised to other dark-matter Lagrangians if desired, with the present choice providing the minimal benchmark required for transparent multi-probe predictions. Extensions to non-canonical scalar sectors or fluid/field effective descriptions can be treated within the same selective-coupling strategy, but are beyond the scope of the present perturbation-benchmark study.

Conservation laws and dark-sector exchange

Since baryons and radiation appear only through minimal couplings in \mathcal{L}_b and \mathcal{L}_{rad} , they satisfy the standard conservation laws,

$$\nabla^\mu T_{\mu\nu}^{(b)} = 0, \quad \nabla^\mu T_{\mu\nu}^{(\text{rad})} = 0. \quad (10)$$

In contrast, the dark sector generally exchanges energy-momentum with the modified gravity sector when $f_T \neq 0$. The non-conservation equation implied by the Bianchi identity and Eq. (6) can be written as [6]

$$\nabla^\mu T_{\mu\nu}^{(\chi)} = \frac{f_T}{\kappa^2 - f_T} \left[\left(T_{\mu\nu}^{(\chi)} + \Theta_{\mu\nu}^{(\chi)} \right) \frac{\nabla^\mu f_T}{f_T} + \nabla^\mu \Theta_{\mu\nu}^{(\chi)} - \frac{1}{2} \nabla_\nu T_\chi \right]. \quad (11)$$

Using Eq. (9), the first term becomes explicitly proportional to $\partial_\mu\chi\partial_\nu\chi$, making the *dark-sector selective* nature of the exchange manifest.

3 Background cosmology

3.1 FLRW setup

We consider a spatially flat FLRW background with cosmic time t ,

$$ds^2 = -dt^2 + a^2(t) \delta_{ij} dx^i dx^j, \quad (12)$$

where $a(t)$ is the scale factor and $H \equiv \dot{a}/a$ is the Hubble rate. For this background,

$$R = 6 \left(2H^2 + \dot{H} \right), \quad (13)$$

and we assume a homogeneous dark-matter field $\chi = \chi(t)$.

The standard background densities of baryons and radiation are denoted by ρ_b and ρ_{rad} , with pressures $p_b \simeq 0$ and $p_{\text{rad}} = \rho_{\text{rad}}/3$. For the canonical field χ , the background energy density and pressure are

$$\rho_\chi = \frac{1}{2}\dot{\chi}^2 + V(\chi), \quad p_\chi = \frac{1}{2}\dot{\chi}^2 - V(\chi), \quad (14)$$

so that $\rho_\chi + p_\chi = \dot{\chi}^2$. The trace defined in Eq. (5) becomes

$$T_\chi = \dot{\chi}^2 - 4V(\chi), \quad (15)$$

and hence $f_R(t)$ and $f_T(t)$ are time dependent through $R(t)$ and $T_\chi(t)$.

3.2 Modified Friedmann equations

Using Eq. (6) and the identity $T_{\mu\nu}^{(\chi)} + \Theta_{\mu\nu}^{(\chi)} = -\partial_\mu\chi\partial_\nu\chi$ from Eq. (9), the 00 component yields

$$3H^2 f_R = \kappa^2 (\rho_b + \rho_{\text{rad}} + \rho_\chi) + f_T \dot{\chi}^2 + \frac{1}{2} (f_R R - f) - 3H \dot{f}_R. \quad (16)$$

The spatial components give

$$-(2\dot{H} + 3H^2) f_R = \kappa^2 (p_{\text{rad}} + p_\chi) - \frac{1}{2} (f_R R - f) + \ddot{f}_R + 2H \dot{f}_R. \quad (17)$$

Combining Eqs. (16) and (17) produces the useful form

$$-2\dot{H} f_R = \kappa^2 [(\rho_b + p_b) + (\rho_{\text{rad}} + p_{\text{rad}}) + (\rho_\chi + p_\chi)] + f_T \dot{\chi}^2 + \ddot{f}_R - H \dot{f}_R, \quad (18)$$

where $p_b \simeq 0$.

Figure 1 makes explicit that the late-time bound on f_{R0} constrains primarily the combination $2\alpha R_0 + \xi T_{\chi 0}$, leading to a degeneracy direction in the $(\hat{\alpha}, \xi)$ plane. In the remainder of the paper we therefore treat the model parameters in a genuinely *multi-probe* way (and, in practice, through normalized parameter combinations): background information alone constrains only limited combinations, whereas growth and lensing respond differently to the scalaron-mediated (curvature) sector and to the selective trace source [3, 4, 8, 16]. Combining $f\sigma_8$ with weak/CMB lensing therefore provides the main route to break this degeneracy at the level of linear perturbations [4, 5, 16].

3.3 Visible-sector conservation and dark-sector evolution

Because baryons and radiation are minimally coupled, Eq. (10) implies the standard continuity equations,

$$\dot{\rho}_b + 3H\rho_b = 0, \quad \dot{\rho}_{\text{rad}} + 4H\rho_{\text{rad}} = 0. \quad (19)$$

The dark sector generally exchanges energy with the modified gravity sector when $f_T \neq 0$ [6]. A convenient way to encode the background dynamics is

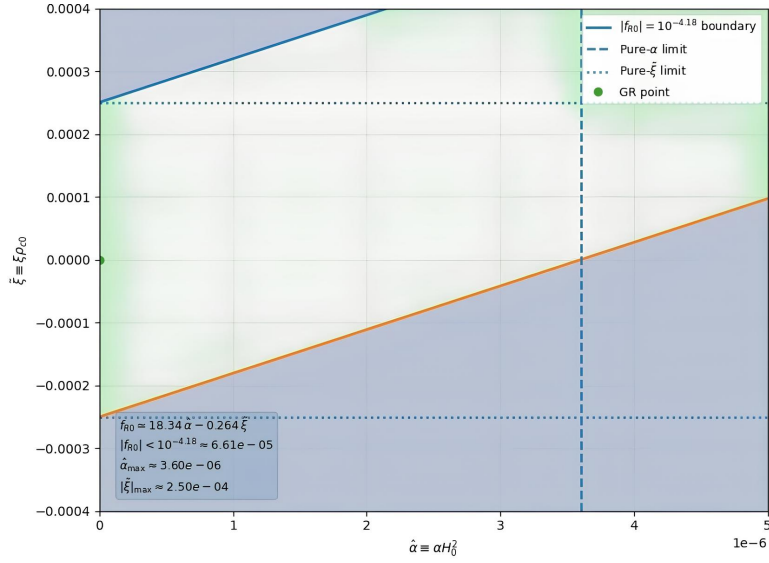


Figure 1: Translated late-time constraint in the $(\hat{\alpha}, \tilde{\xi})$ plane for the polynomial model $f(R, T_\chi) = R + \alpha R^2 + \xi R T_\chi + \beta T_\chi^2$, using the benchmark cap $\log_{10} |f_{R0}| < -4.18$ and the dust-level approximation $T_{\chi 0} \simeq -\rho_{\chi 0}$. Here $\hat{\alpha} \equiv \alpha H_0^2$ and $\tilde{\xi} \equiv \xi \rho_{c0}$. The shaded strip shows the allowed region satisfying $|f_{R0}| = |2\alpha R_0 + \xi T_{\chi 0}| < 10^{-4.18}$, illustrating the parameter-combination degeneracy beyond the pure- α and pure- ξ limits (dashed/dotted lines).

through the modified equation of motion obtained by varying the action with respect to χ . Denoting $V_{,\chi} \equiv dV/d\chi$, the homogeneous field satisfies

$$\left(1 + \frac{f_T}{\kappa^2}\right) (\ddot{\chi} + 3H\dot{\chi}) + \frac{\dot{f}_T}{\kappa^2} \dot{\chi} + \left(1 + \frac{2f_T}{\kappa^2}\right) V_{,\chi} = 0. \quad (20)$$

Equivalently, the dark-matter energy density obeys a modified continuity equation,

$$\dot{\rho}_\chi + 3H(\rho_\chi + p_\chi) = Q_\chi, \quad (21)$$

where, using Eq. (20),

$$Q_\chi = \dot{\chi}(\ddot{\chi} + 3H\dot{\chi} + V_{,\chi}) = -\frac{\dot{f}_T}{\kappa^2 + f_T} \dot{\chi}^2 - \frac{f_T}{\kappa^2 + f_T} V_{,\chi} \dot{\chi}. \quad (22)$$

This term quantifies the background-level energy exchange induced by the selective trace coupling.

3.4 Consistency conditions and GR limit

The General Relativity limit is recovered when $f(R, T_\chi) \rightarrow R$ so that $f_R \rightarrow 1$ and $f_T \rightarrow 0$, in which case Eqs. (16)–(22) reduce to the standard Friedmann system with a canonical scalar field. For a well-defined background evolution, the theory must also avoid singular denominators, in particular $\kappa^2 \pm f_T \neq 0$ wherever Eqs. (11) and (22) are used, and it must satisfy the usual positivity requirement $f_R > 0$ to prevent an effective sign flip of the gravitational coupling [10, 20].

Viability and stability cuts. In addition to the GR limit and the absence of singular denominators, we impose linear-viability conditions for a predictive late-time cosmology:

$$f_R > 0, \quad f_{RR} > 0, \quad K \equiv 1 + \frac{f_T}{\kappa^2} > 0, \quad (23)$$

where $f_{RR} > 0$ ensures Dolgov–Kawasaki stability in the curvature sector [21, 10, 20] and $K > 0$ guarantees that the coefficient of $\delta\ddot{\chi}$ in the perturbed Klein–Gordon equation (Eq. 46) remains positive, avoiding ghost-like kinetic behavior of χ fluctuations.

Effective dust regime of χ . Although the selective trace source is defined using a canonical scalar field χ , the late-time large-scale observables considered here are most directly interpreted when the dark sector clusters effectively as pressureless matter. This is consistently realized, for instance, by an oscillating scalar in an approximately quadratic potential in the regime $m_\chi \gg H$, for which time-averaging yields $\langle w_\chi \rangle \simeq 0$ and hence $\langle T_\chi \rangle \simeq -\langle \rho_\chi \rangle$ (up to corrections suppressed by H/m_χ) [22, 17, 18]. In this limit, the standard growth equation

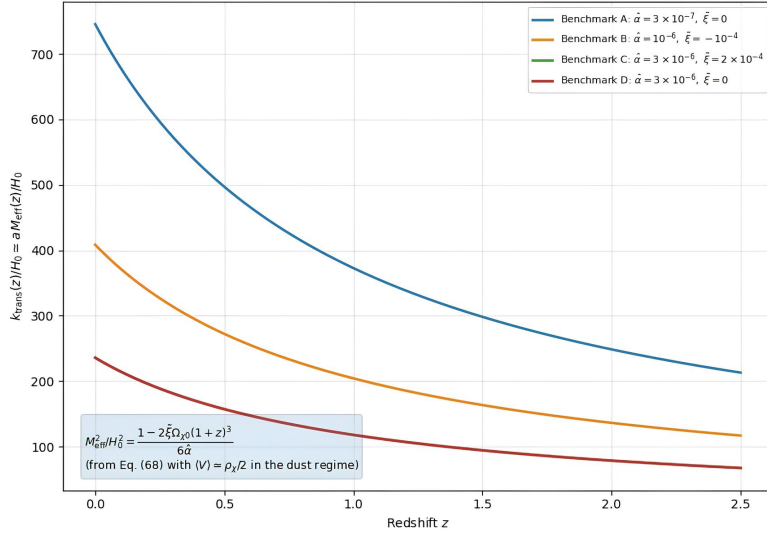


Figure 2: Redshift evolution of the quasi-static transition scale $k_{\text{trans}}(z) \simeq a M_{\text{eff}}(z)$ for viable benchmark points in the $(\hat{\alpha}, \tilde{\xi})$ plane, using the polynomial model $f(R, T_\chi) = R + \alpha R^2 + \xi R T_\chi + \beta T_\chi^2$ and the effective mass expression in Eq. (68). The plotted curves use the dust-regime benchmark closure $\langle V \rangle \simeq \rho_\chi/2$ (oscillating quadratic scalar), yielding $M_{\text{eff}}^2/H_0^2 = [1 - 2\tilde{\xi}\Omega_{\chi 0}(1+z)^3]/(6\hat{\alpha})$. This figure identifies the scale at which scalaron-mediated modifications are expected to transition in the quasi-static regime [10, 22].

used in Sec. 5 applies, while the selective coupling effects enter through $(f_T, \delta f_T)$ and the additional source terms derived in Sec. 4.

More precisely, the dust-like closure adopted here assumes that the background field oscillates around a locally quadratic minimum, $V(\chi) \simeq \frac{1}{2}m_\chi^2\chi^2$, with oscillation frequency m_χ much larger than the Hubble rate over the late-time redshift range relevant to the linear observables considered. In this adiabatic/averaged regime, residual pressure and gradient contributions are suppressed on sufficiently large scales [22, 18]. Correspondingly, the perturbation-level mapping developed here is formulated for the late-time large-scale linear regime in which the oscillation-averaged effective dust approximation is valid. Within this regime, the standard dust-based variable $f\sigma_8$ can be used consistently in the linear observational mapping employed in Sec. 5. The present construction therefore targets the perturbation-level, late-time large-scale sector, while preserving the selective-coupling modifications through $(f_T, \delta f_T)$ and the extra source terms derived in Sec. 4.

4 Linear cosmological perturbations

4.1 Newtonian gauge and perturbation variables

We work with scalar perturbations around the flat FLRW background in Newtonian gauge [23],

$$ds^2 = -(1 + 2\Psi) dt^2 + a^2(t)(1 - 2\Phi) \delta_{ij} dx^i dx^j, \quad (24)$$

where $\Psi(t, \mathbf{x})$ and $\Phi(t, \mathbf{x})$ are the Bardeen potentials. The dark-matter field is decomposed as

$$\chi(t, \mathbf{x}) = \bar{\chi}(t) + \delta\chi(t, \mathbf{x}), \quad (25)$$

and similarly for all background quantities. We denote Fourier modes by $\delta X(t, \mathbf{x}) = \int \frac{d^3k}{(2\pi)^3} \delta X(t, \mathbf{k}) e^{i\mathbf{k}\cdot\mathbf{x}}$.

For later use, we define the total (visible + dark) matter density perturbation by $\delta\rho \equiv \delta\rho_b + \delta\rho_{\text{rad}} + \delta\rho_\chi$, and introduce the velocity potentials v_I (for each species I) through $\delta u_i^{(I)} = \partial_i v_I$ at linear order.

4.2 Perturbations of T_χ and of the coupling functions

The trace T_χ defined in Eq. (5) perturbs as $T_\chi = \bar{T}_\chi + \delta T_\chi$. For the canonical scalar field in Newtonian gauge, keeping only linear terms, one finds

$$\delta T_\chi = 2\dot{\bar{\chi}} \delta\dot{\chi} - 2\Psi \dot{\bar{\chi}}^2 - 4V_{,\chi} \delta\chi, \quad (26)$$

where $V_{,\chi} \equiv dV/d\chi$ is evaluated on the background.

Since f_R and f_T depend on (R, T_χ) , their perturbations are

$$\delta f_R = f_{RR} \delta R + f_{RT} \delta T_\chi, \quad (27)$$

$$\delta f_T = f_{TR} \delta R + f_{TT} \delta T_\chi, \quad (28)$$

where $f_{RR} \equiv \partial^2 f / \partial R^2$, $f_{RT} \equiv \partial^2 f / (\partial R \partial T_\chi)$, and $f_{TT} \equiv \partial^2 f / \partial T_\chi^2$ are evaluated on the background. The Ricci-scalar perturbation δR is obtained from Eq. (24) and will enter the linearized field equations through Eqs. (27)–(28). For concreteness and parameter-level interpretability, we adopt the minimal polynomial realization

$$f(R, T_\chi) = R + \alpha R^2 + \xi R T_\chi + \beta T_\chi^2, \quad (29)$$

as an effective expansion around the GR limit. These relations also clarify the parameter roles at linear order in this parametrization: α enters primarily through the curvature-response sector (via f_{RR} and the effective scalaron scale), ξ mixes curvature and dark-sector trace perturbations through $f_{RT} = f_{TR}$, and β controls the leading trace-sector response through f_{TT} . As a result, different observables probe different combinations of (α, ξ, β) : background information alone is generally insufficient to separate them, whereas growth and lensing respond differently to the curvature and trace-coupling channels [8, 4, 16].

4.3 Effective functions for growth and lensing

A key objective is to connect the linearized system to perturbation-sensitive observables. In Fourier space, and in the sub-horizon regime, the scalar sector can be parameterized by effective modified-gravity functions $\mu(k, a)$ and $\eta(k, a)$ defined via [16, 4]

$$k^2 \Psi \equiv -4\pi G a^2 \mu(k, a) \rho_m \Delta_m, \quad \eta(k, a) \equiv \frac{\Phi}{\Psi}, \quad (30)$$

where ρ_m is the background total matter density (typically baryons plus the clustering dark component), and Δ_m is the gauge-invariant comoving matter density contrast [23].

No double counting between $\rho_m \Delta_m$ and Π_{DS} . In our notation, $\rho_m \Delta_m$ denotes the standard comoving clustering source entering the phenomenological definitions of μ and Σ , including the clustering dark component in the effective dust regime. The additional term Π_{DS} introduced in the QS Poisson constraint (Eq. 60) collects only the selective trace-coupling contributions proportional to $(f_T, \delta f_T)$ and vanishes in the GR limit $f_T \rightarrow 0$; therefore Π_{DS} should be interpreted as an extra modified-gravity source, not as a second counting of the matter density perturbation.

The Weyl (lensing) potential is controlled by $\Phi + \Psi$, and it is convenient to define [16, 4]

$$k^2(\Phi + \Psi) \equiv -8\pi G a^2 \Sigma(k, a) \rho_m \Delta_m, \quad \Sigma(k, a) \equiv \frac{\mu(k, a)}{2} [1 + \eta(k, a)]. \quad (31)$$

In the following subsections we derive the full linearized equations from Eq. (6) and identify $\mu(k, a)$ and $\eta(k, a)$ explicitly in terms of the model functions and background evolution, enabling direct confrontation with redshift-space distortions (via $f\sigma_8$) and lensing data.

4.4 Perturbed dark-matter stress–energy

For the canonical field χ defined in Eq. (3), the linear perturbations of energy density, pressure, and momentum density in Newtonian gauge are [23, 24]

$$\delta\rho_\chi = \dot{\bar{\chi}}\delta\dot{\chi} - \dot{\bar{\chi}}^2\Psi + V_{,\chi}\delta\chi, \quad (32)$$

$$\delta p_\chi = \dot{\bar{\chi}}\delta\dot{\chi} - \dot{\bar{\chi}}^2\Psi - V_{,\chi}\delta\chi, \quad (33)$$

$$\delta T_{0i}^{(\chi)} = -\dot{\bar{\chi}}\partial_i\delta\chi \quad \Rightarrow \quad (\bar{\rho}_\chi + \bar{p}_\chi)v_\chi = -\dot{\bar{\chi}}\delta\chi, \quad (34)$$

where $V_{,\chi} \equiv dV/d\chi$ is evaluated on the background.

4.5 Linearized field equations and robust slip relation

Define the geometric operator

$$\mathcal{E}_{\mu\nu} \equiv f_R R_{\mu\nu} - \frac{1}{2}f g_{\mu\nu} + (g_{\mu\nu}\square - \nabla_\mu\nabla_\nu)f_R. \quad (35)$$

The field equations (6) can be written compactly as

$$\mathcal{E}_{\mu\nu} = \kappa^2 \left(T_{\mu\nu}^{(b)} + T_{\mu\nu}^{(\text{rad})} + T_{\mu\nu}^{(\chi)} \right) - f_T S_{\mu\nu}, \quad S_{\mu\nu} \equiv T_{\mu\nu}^{(\chi)} + \Theta_{\mu\nu}^{(\chi)}. \quad (36)$$

For canonical χ , Eq. (9) implies the exact identity

$$S_{\mu\nu} = -\partial_\mu\chi\partial_\nu\chi. \quad (37)$$

At the background level one has $\bar{S}_{00} = -\dot{\bar{\chi}}^2$ and $\bar{S}_{0i} = \bar{S}_{ij} = 0$. At linear order this gives the particularly simple perturbations

$$\delta S_{00} = -2\dot{\bar{\chi}}\delta\dot{\chi}, \quad \delta S_{0i} = -\dot{\bar{\chi}}\partial_i\delta\chi, \quad \delta S_{ij} = 0 \quad (\text{to first order}). \quad (38)$$

Therefore, the linearized field equations take the schematic but exact form

$$\delta\mathcal{E}_{\mu\nu} = \kappa^2 \delta T_{\mu\nu}^{(\text{tot})} - \bar{f}_T \delta S_{\mu\nu} - \delta f_T \bar{S}_{\mu\nu}, \quad (39)$$

where $\delta T_{\mu\nu}^{(\text{tot})}$ includes baryons, radiation, and χ .

A key robust consequence follows from the traceless spatial (ij) sector. Since $\delta S_{ij} = 0$ at linear order and the canonical scalar has no anisotropic stress, the traceless ij equation yields the gravitational slip sourced purely by δf_R [10, 20],

$$\Phi - \Psi = \frac{\delta f_R}{\bar{f}_R}. \quad (40)$$

In the next subsection we will compute the explicit 00 and 0*i* components of Eq. (39) in Fourier space and then extract $\mu(k, a)$ and $\eta(k, a)$ consistently with Eqs. (30)–(31).

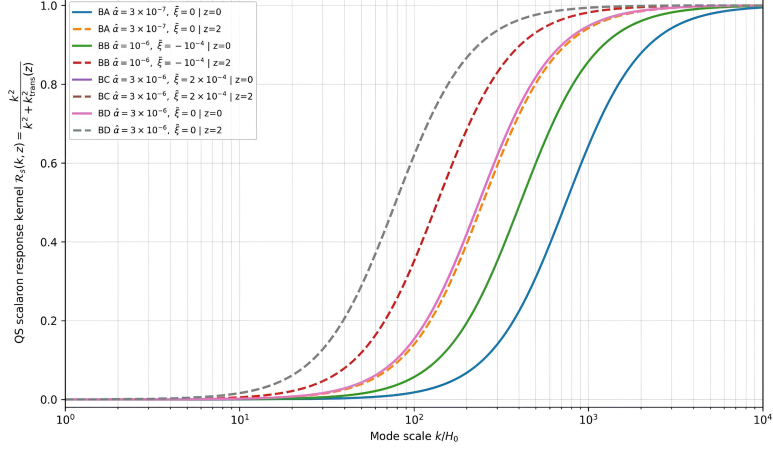


Figure 3: Diagnostic quasi-static scalaron response kernel, $\mathcal{R}_s(k, z) = k^2/[k^2 + k_{\text{trans}}^2(z)]$, for viable benchmark points of the selective dark-sector $f(R, T_\chi)$ model, where $k_{\text{trans}}(z) \simeq a M_{\text{eff}}(z)$ is determined by the effective mass derived in Sec. 4.11. Solid (dashed) curves denote $z = 0$ ($z = 2$). This plot isolates the scale at which scalaron-mediated modifications become active and provides a theory-level bridge between the effective-mass sector and the scale-dependent growth/lensing observables reconstructed in the quasi-static regime.

4.6 Linearized modified Klein–Gordon equation

The dark-matter field equation follows from varying the action with respect to χ . It is convenient to introduce the dimensionless coupling

$$B \equiv \frac{f_T}{\kappa^2}, \quad \mathcal{K} \equiv 1 + B, \quad \mathcal{C} \equiv 1 + 2B, \quad (41)$$

so that the exact covariant equation of motion can be written as

$$\mathcal{K} \square \chi + \nabla_\mu B \nabla^\mu \chi - \mathcal{C} V_{,\chi} = 0. \quad (42)$$

On the FLRW background this reproduces Eq. (20).

Linearizing Eq. (42) around $\chi = \bar{\chi} + \delta\chi$ and $B = \bar{B} + \delta B$ yields, to first order,

$$\bar{\mathcal{K}} \delta(\square \chi) + \delta \mathcal{K} \square \bar{\chi} + \nabla_\mu \delta B \nabla^\mu \bar{\chi} + \nabla_\mu \bar{B} \nabla^\mu \delta \chi + \delta g^{\mu\nu} (\partial_\mu \bar{B})(\partial_\nu \bar{\chi}) - \bar{\mathcal{C}} V_{,\chi} \delta \chi - \delta \mathcal{C} V_{,\chi} = 0, \quad (43)$$

where $\delta \mathcal{K} = \delta B$ and $\delta \mathcal{C} = 2 \delta B$.

The coupling perturbation δB is determined by the gravitational function through

$$\delta B = \frac{1}{\kappa^2} \delta f_T = \frac{1}{\kappa^2} (f_{TR} \delta R + f_{TT} \delta T_\chi), \quad (44)$$

with δT_χ given in Eq. (26). On the FLRW background, $\delta g^{00} = 2\Psi$ and

$$\delta g^{\mu\nu} (\partial_\mu \bar{B})(\partial_\nu \bar{\chi}) = 2\Psi \dot{\bar{B}} \dot{\bar{\chi}}. \quad (45)$$

Finally, the perturbed d'Alembertian acting on χ is defined geometrically by

$$\delta(\square\chi) \equiv \delta(g^{\mu\nu}\nabla_\mu\nabla_\nu\chi) = \bar{\square}\delta\chi + \delta g^{\mu\nu}\bar{\nabla}_\mu\bar{\nabla}_\nu\bar{\chi} + \bar{g}^{\mu\nu}\delta\Gamma^\rho{}_{\mu\nu}\partial_\rho\bar{\chi}, \quad (46)$$

which can be evaluated explicitly in Newtonian gauge using Eq. (24). In the next subsection we provide the explicit Fourier-space form and then close the system for $(\Phi, \Psi, \delta\chi)$ to extract $\mu(k, a)$ and $\eta(k, a)$ consistently with Eqs. (30)–(31).

4.7 Explicit Newtonian-gauge form and Fourier-space equation for $\delta\chi$

Explicit form of $\delta(\square\chi)$

Evaluating Eq. (46) for the Newtonian-gauge metric (24) and a homogeneous background $\bar{\chi}(t)$ gives

$$\delta(\square\chi) = -\delta\ddot{\chi} - 3H\delta\dot{\chi} - \frac{k^2}{a^2}\delta\chi + \dot{\chi}\left(\dot{\Psi} + 3\dot{\Phi}\right) + 2\Psi\left(\ddot{\chi} + 3H\dot{\chi}\right), \quad (47)$$

where k is the comoving wavenumber in Fourier space.

Fourier-space linearized modified Klein–Gordon equation

Using Eq. (47) in the compact linear equation (43), and keeping the definitions $\mathcal{K} = 1 + B$, $\mathcal{C} = 1 + 2B$ from Eq. (41), one obtains

$$\bar{\mathcal{K}}\delta\ddot{\chi} + \left(3H\bar{\mathcal{K}} + \dot{B}\right)\delta\dot{\chi} + \left(\bar{\mathcal{K}}\frac{k^2}{a^2} + \bar{\mathcal{C}}V_{,xx}\right)\delta\chi = \bar{\mathcal{K}}\dot{\chi}\left(\dot{\Psi} + 3\dot{\Phi}\right) - 2\bar{\mathcal{C}}V_{,x}\Psi - \dot{\chi}\delta\dot{B} + \delta B\bar{\square}\chi - 2V_{,x}\delta B, \quad (48)$$

where

$$\bar{\square}\chi = -(\ddot{\chi} + 3H\dot{\chi}), \quad (49)$$

and the coupling perturbation δB is

$$\delta B = \frac{1}{\kappa^2}(f_{TR}\delta R + f_{TT}\delta T_\chi), \quad \delta T_\chi = 2\dot{\chi}\delta\dot{\chi} - 2\Psi\dot{\chi}^2 - 4V_{,x}\delta\chi, \quad (50)$$

with all background-dependent coefficients evaluated on (\bar{R}, \bar{T}_χ) . Equation (48) closes the $\delta\chi$ dynamics once δR is specified from the metric perturbations.

4.8 Eliminating δR and closing the system

A practical advantage of the (R, T_χ) dependence is that δR never needs to be written explicitly in terms of (Φ, Ψ) in order to close the system. From Eqs. (27)–(28) we have, at linear order,

$$\delta f_R = f_{RR}\delta R + f_{RT}\delta T_\chi, \quad \delta f_T = f_{TR}\delta R + f_{TT}\delta T_\chi, \quad (51)$$

with $f_{RT} = f_{TR}$. We assume $f_{RR} \neq 0$ so that δR can be eliminated in favor of δf_R ; the special case $f_{RR} = 0$ can be treated separately. Solving the first relation for δR gives

$$\delta R = \frac{1}{f_{RR}} (\delta f_R - f_{RT} \delta T_\chi). \quad (52)$$

Substituting Eq. (52) into δf_T yields an expression that depends only on δf_R and δT_χ ,

$$\delta f_T = \frac{f_{RT}}{f_{RR}} \delta f_R + \left(f_{TT} - \frac{f_{RT}^2}{f_{RR}} \right) \delta T_\chi. \quad (53)$$

Therefore the coupling perturbation $\delta B = \delta f_T / \kappa^2$ becomes

$$\delta B = \frac{1}{\kappa^2} \frac{f_{RT}}{f_{RR}} \delta f_R + \frac{1}{\kappa^2} \left(f_{TT} - \frac{f_{RT}^2}{f_{RR}} \right) \delta T_\chi. \quad (54)$$

Using the robust slip relation (40),

$$\delta f_R = \bar{f}_R (\Phi - \Psi), \quad (55)$$

Eq. (54) can be expressed entirely in terms of (Φ, Ψ) and δT_χ . For reference, the canonical-field trace perturbation is

$$\delta T_\chi = 2\dot{\chi} \delta\dot{\chi} - 2\Psi \dot{\chi}^2 - 4V_{,\chi} \delta\chi. \quad (56)$$

4.9 Trace equation for the scalaron perturbation δf_R

Taking the trace of the field equations (6) gives the exact scalar equation

$$3\Box f_R + f_{RR} R - 2f = \kappa^2 T^{(\text{tot})} - f_T S, \quad S \equiv g^{\mu\nu} (T_{\mu\nu}^{(\chi)} + \Theta_{\mu\nu}^{(\chi)}) = -(\partial\chi)^2, \quad (57)$$

where $T^{(\text{tot})}$ is the trace of the total stress-energy tensor (baryons + radiation + χ). Linearizing Eq. (57) yields

$$3\delta(\Box f_R) + \bar{R} \delta f_R - \bar{f}_R \delta R - 2\bar{f}_T \delta T_\chi = \kappa^2 \delta T^{(\text{tot})} - \bar{f}_T \delta S - \delta f_T \bar{S}, \quad (58)$$

with δR eliminated by Eq. (52) and δf_T given by Eq. (53). For the canonical field,

$$\bar{S} = \dot{\chi}^2, \quad \delta S = 2\dot{\chi} \delta\dot{\chi} - 2\Psi \dot{\chi}^2. \quad (59)$$

Finally, the perturbed d'Alembertian acting on f_R is defined analogously to Eq. (46) as

$$\delta(\Box f_R) = \bar{\Box} \delta f_R + \delta g^{\mu\nu} \bar{\nabla}_\mu \bar{\nabla}_\nu \bar{f}_R + \bar{g}^{\mu\nu} \delta\Gamma^\rho_{\mu\nu} \partial_\rho \bar{f}_R, \quad (60)$$

where $\bar{f}_R = \bar{f}_R(t)$ in the background.

Equations (48), (58), and (40), together with Eq. (54), provide a gauge-consistent closure once supplemented by the 00 and 0i constraint equations for the metric potentials.

4.10 Quasi-static sub-horizon limit and observable reconstruction

We now specialize to the quasi-static (QS) sub-horizon regime [10, 8],

$$\frac{k^2}{a^2} \gg H^2, \quad |\dot{\Phi}|, |\dot{\Psi}| \ll \frac{k}{a} |\Phi|, \frac{k}{a} |\Psi|, \quad |\delta \dot{f}_R| \ll \frac{k}{a} |\delta f_R|, \quad (61)$$

retaining the leading spatial-gradient terms that control growth and lensing.

QS constraints for the metric potentials

In the QS limit, the linearized field equations (39) reduce to a Poisson-type constraint for Φ with two distinct sources: (i) the standard clustering source $\rho_m \Delta_m$ and (ii) a dark-sector selective contribution induced by $(f_T, \delta f_T)$ and δS_{00} . We write the leading-gradient constraint in the compact form

$$\frac{k^2}{a^2} \Phi \simeq -\frac{\kappa^2}{2\bar{f}_R} \rho_m \Delta_m - \frac{1}{2\bar{f}_R} \Pi_{\text{DS}}(k, a) - \frac{k^2}{2a^2} \frac{\delta f_R}{\bar{f}_R}, \quad (62)$$

where Π_{DS} collects the dark-sector selective terms that vanish in the GR limit and is given by

$$\Pi_{\text{DS}}(k, a) \equiv \dot{\chi}^2 \delta f_T - \bar{f}_T \delta S_{00}, \quad \delta S_{00} = -2\dot{\chi} \delta \dot{\chi}. \quad (63)$$

The coupling perturbation δf_T is eliminated by Eq. (53), so that Π_{DS} is expressed entirely in terms of δf_R and $(\delta\chi, \delta\dot{\chi})$.

The gravitational slip remains exact at linear order,

$$\Phi - \Psi = \frac{\delta f_R}{\bar{f}_R}, \quad (64)$$

so that Ψ is obtained from Φ once δf_R is known.

QS trace equation for δf_R

In the same QS limit, the trace equation (58) becomes an algebraic relation that determines δf_R up to the source terms. Keeping the dominant gradient term $\delta(\square f_R) \simeq -(k^2/a^2)\delta f_R$ and eliminating δR and δf_T using Eqs. (52) and (53), we obtain the schematic QS form

$$\left(\frac{k^2}{a^2} + m_f^2(a)\right) \delta f_R \simeq \mathcal{S}_{\text{tot}}(k, a) + \mathcal{S}_{\text{DS}}(k, a), \quad (65)$$

where $m_f^2(a)$ is the effective mass term for the scalaron perturbation δf_R and \mathcal{S}_{tot} and \mathcal{S}_{DS} denote, respectively, the standard trace source (from $\delta T^{(\text{tot})}$) and the additional dark-sector selective sources involving δT_χ and δS . Their explicit expressions follow uniquely once a concrete model $f(R, T_\chi)$ is specified, because they depend only on the background derivatives $(\bar{f}_R, \bar{f}_{RR}, \bar{f}_{RT}, \bar{f}_T, \bar{f}_{TT})$ and on the perturbations $(\delta\chi, \delta\dot{\chi}, \Phi, \Psi)$.

Reconstruction of $\mu(k, a)$, $\eta(k, a)$ and $\Sigma(k, a)$

Given δf_R from Eq. (65), the potentials are obtained from Eqs. (62) and (64), and the observable functions are then read off from their defining relations (30)–(31):

$$\mu(k, a) = -\frac{k^2 \Psi}{4\pi G a^2 \rho_m \Delta_m}, \quad \eta(k, a) = \frac{\Phi}{\Psi}, \quad \Sigma(k, a) = -\frac{k^2(\Phi + \Psi)}{8\pi G a^2 \rho_m \Delta_m}. \quad (66)$$

In the GR limit $\bar{f}_R \rightarrow 1$ and $\Pi_{\text{DS}} \rightarrow 0$ and $\delta f_R \rightarrow 0$, one recovers $\mu = \eta = \Sigma = 1$.

4.11 QS scalaron equation and effective mass

In the QS sub-horizon regime, the trace equation provides an algebraic relation for the scalaron perturbation δf_R . Keeping the dominant gradient contribution $\delta(\square f_R) \simeq -(k^2/a^2)\delta f_R$ and eliminating δR and δf_T using Eqs. (52) and (53), one may cast the result in the compact form

$$\left(\frac{k^2}{a^2} + M_{\text{eff}}^2(a)\right) \delta f_R \simeq -\frac{1}{3} \left[\kappa^2 \delta T^{(\text{tot})} - \bar{f}_T \delta S - \mathcal{B}(a) \delta T_\chi \right], \quad (67)$$

where the effective mass and the explicit δT_χ -source coefficient are determined only by background derivatives of $f(R, T_\chi)$:

$$M_{\text{eff}}^2(a) \equiv \frac{\bar{f}_R - \bar{R} \bar{f}_{RR} - \bar{S} \bar{f}_{RT}}{3 \bar{f}_{RR}} = \frac{1}{3} \left[\frac{\bar{f}_R - \bar{S} \bar{f}_{RT}}{\bar{f}_{RR}} - \bar{R} \right], \quad \mathcal{B}(a) \equiv \bar{f}_R \frac{\bar{f}_{RT}}{\bar{f}_{RR}} - 2 \bar{f}_T + \bar{S} \left(\bar{f}_{TT} - \frac{\bar{f}_{RT}^2}{\bar{f}_{RR}} \right). \quad (68)$$

For the canonical field, $\bar{S} = \dot{\bar{\chi}}^2$ and $\bar{T}_\chi = \bar{S} - 4V(\bar{\chi})$, hence the coefficient $\mathcal{B}(a)$ and the explicit δT_χ -source contribution in Eq. (67) are fully determined by background derivatives of $f(R, T_\chi)$ together with the canonical scalar-sector perturbations under the QS sub-horizon approximation.

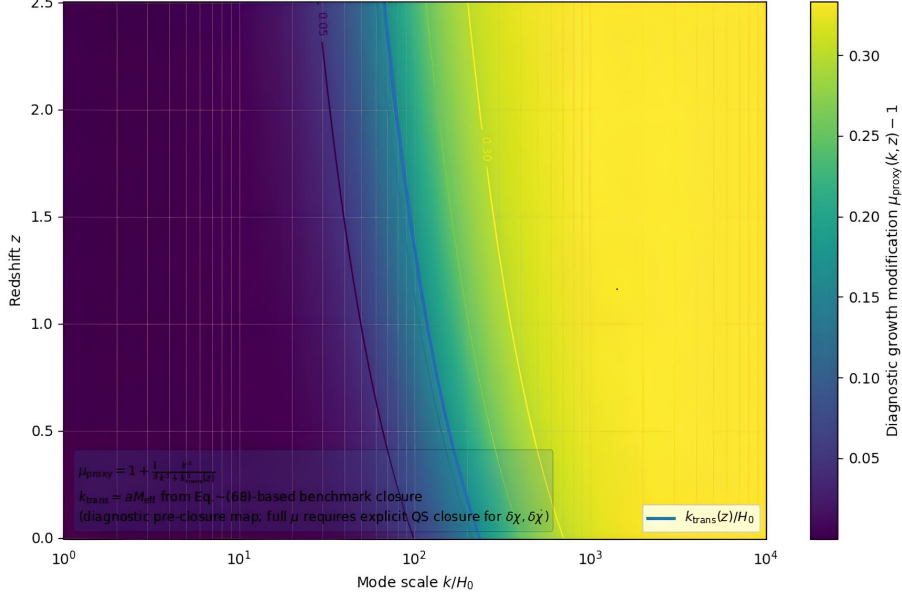


Figure 4: **Diagnostic QS growth-modification map and transition scale.** Two-dimensional map of the diagnostic growth modification $\mu_{\text{proxy}}(k, z) - 1$ in the quasi-static sub-horizon regime, displayed over mode scale k/H_0 and redshift z . The proxy $\mu_{\text{proxy}}(k, z)$ is constructed from the QS algebraic closure for the scalaron perturbation in Eq. (67) with the background-defined coefficients $M_{\text{eff}}(a)$ and $\mathcal{B}(a)$ given in Eq. (68). The solid curve shows the evolving transition locus $k_{\text{trans}}(z)/H_0$, illustrating that the onset of scale-dependent growth departures tracks the effective-mass scale $k_{\text{trans}}(z) \simeq aM_{\text{eff}}(z)$. This figure therefore provides a compact pre-closure diagnostic of where, in the (k, z) plane, the model predicts the strongest QS growth response.

$$\delta S = 2\dot{\chi} \delta\dot{\chi} - 2\Psi \dot{\chi}^2, \quad \delta T_\chi = \delta S - 4V_{,\chi} \delta\chi = 2\dot{\chi} \delta\dot{\chi} - 2\Psi \dot{\chi}^2 - 4V_{,\chi} \delta\chi. \quad (69)$$

For the specific polynomial choice in Eq. (29), using $\bar{f}_{RR} = 2\alpha$, $\bar{f}_{RT} = \xi$, $\bar{f}_{TT} = 2\beta$ and $\bar{f}_R = 1 + 2\alpha\bar{R} + \xi\bar{T}_\chi$, one obtains the explicit background functions

$$M_{\text{eff}}^2(a) = \frac{1}{3} \left[\frac{1 + 2\alpha\bar{R} + \xi\bar{T}_\chi - \xi\bar{S}}{2\alpha} - \bar{R} \right] = \frac{1}{3} \left[\frac{1 + \xi(\bar{T}_\chi - \bar{S})}{2\alpha} \right] = \frac{1 - 4\xi V(\bar{\chi})}{6\alpha}, \quad (70)$$

and

$$\mathcal{B}(a) = (1 + 2\alpha\bar{R} + \xi\bar{T}_\chi) \frac{\xi}{2\alpha} - 2(\xi\bar{R} + 2\beta\bar{T}_\chi) + \dot{\chi}^2 \left(2\beta - \frac{\xi^2}{2\alpha} \right). \quad (71)$$

Equation (67), together with the QS constraints (62) and the slip relation (64), enables a fully explicit reconstruction of $\mu(k, a)$, $\eta(k, a)$, and $\Sigma(k, a)$ once the perturbations $(\delta\chi, \delta\dot{\chi})$ are related to $\rho_m \Delta_m$ via the QS limit of Eq. (48) with δB from Eq. (44).

5 Observational signatures and inference strategy

5.1 Background expansion observables

Although we work in natural units ($c = \hbar = 1$) in the theoretical sections, in this section we restore c when expressing observational distances in conventional units. Assuming spatial flatness, we compute

$$D_H(z) = \frac{c}{H(z)}, \quad D_M(z) = c \int_0^z \frac{dz'}{H(z')}, \quad D_L(z) = (1+z) D_M(z), \quad (72)$$

and the corresponding distance modulus for Type Ia supernovae [25],

$$\mu_{\text{SN}}(z) = 5 \log_{10} \left[\frac{D_L(z)}{\text{Mpc}} \right] + 25. \quad (73)$$

For BAO analyses we adopt the standard volume-averaged distance

$$D_V(z) = [z D_M^2(z) D_H(z)]^{1/3}, \quad (74)$$

and/or the anisotropic pair $(D_M(z)/r_d, D_H(z)/r_d)$, where r_d is the sound horizon at the drag epoch computed consistently within the same background cosmology [26, 27].

5.2 Linear growth and lensing in the QS regime

On sub-horizon scales where the QS approximation holds, clustering and lensing are controlled by the effective functions $\mu(k, a)$ and $\Sigma(k, a)$ defined in Eqs. (30) and (31) [10, 8, 4]. For each Fourier mode k , the growth of the comoving density contrast $\Delta_m(k, a)$ can be written as

$$\Delta_m'' + \left(2 + \frac{H'}{H} \right) \Delta_m' - \frac{3}{2} \Omega_m(a) \mu(k, a) \Delta_m = 0, \quad (75)$$

where primes denote derivatives with respect to $\ln a$ and $\Omega_m(a) \equiv \kappa^2 \rho_m / (3H^2)$. Redshift-space distortions constrain $f\sigma_8(z)$ with

$$f(z) \equiv \frac{d \ln \Delta_m}{d \ln a}, \quad f\sigma_8(z) = f(z) \sigma_8(z), \quad (76)$$

while weak lensing and CMB lensing constrain the Weyl potential through $\Sigma(k, a)$,

$$k^2(\Phi + \Psi) = -8\pi G a^2 \Sigma(k, a) \rho_m \Delta_m. \quad (77)$$

In our framework, μ , η and Σ are reconstructed from Eqs. (62), (64), and (66), using δf_R obtained from the QS trace equation (67) and the model derivatives in Sec. 2.

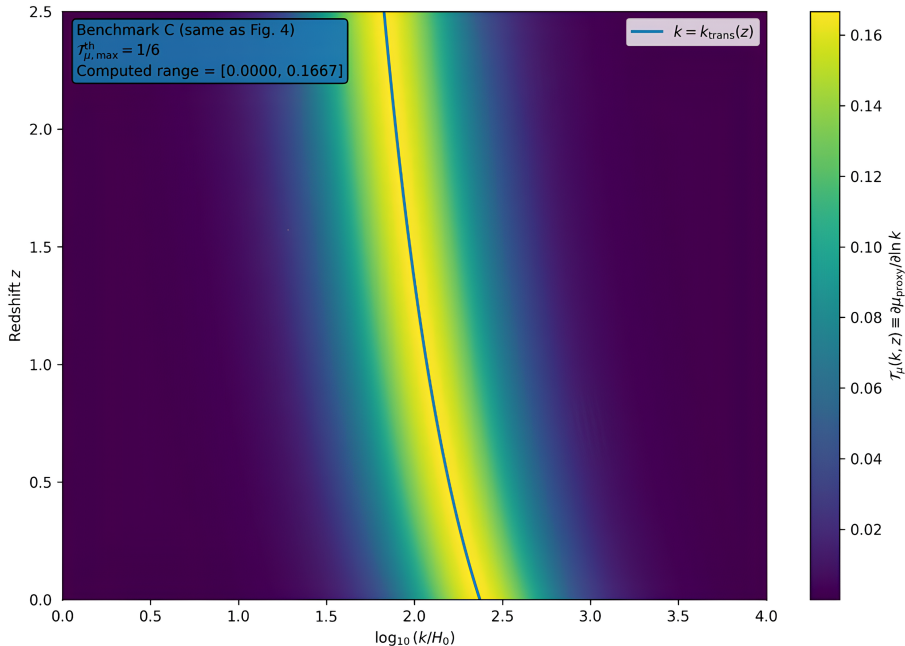


Figure 5: **Transition-sensitivity ridge of the quasi-static (QS) growth diagnostic.** Heat map of the logarithmic response measure $\mathcal{T}_\mu(k, z) \equiv \partial\mu_{\text{proxy}}(k, z)/\partial \ln k$ across the (k, z) plane (horizontal axis: $\log_{10}(k/H_0)$; vertical axis: redshift z), for the same Benchmark C setup adopted in the preceding analysis. The bright ridge delineates the scale band where the reconstructed QS growth response becomes maximally sensitive to mode scale, marking the effective transition between GR-like behavior and the modified-gravity scalar sector in the QS limit. The solid curve overlays the predicted transition locus $k = k_{\text{trans}}(z)$, highlighting that the strongest scale sensitivity tracks the evolving QS transition scale inferred from the effective-mass sector. The color bar reports the computed range of \mathcal{T}_μ for this benchmark.

Figure 5 visualizes where the QS reconstruction becomes most scale-sensitive in the (k, z) plane, and shows that the resulting sensitivity ridge follows the transition locus $k_{\text{trans}}(z)$ identified from the effective-mass sector.

5.3 Data vector design for multi-probe inference

We define an implementation-ready multi-probe data-vector structure designed to separately test (i) the background expansion and (ii) the growth and lensing

sector:

$$\mathcal{D} = \{\text{BAO}, \text{SN}, f\sigma_8, \text{WL}, \text{CMB lensing}\}. \quad (78)$$

Geometric probes (BAO+SN) mainly constrain $H(z)$ and distances, while late-time clustering and lensing probe the scale and time dependence of $\mu(k, a)$ and $\Sigma(k, a)$ in the linear regime. As representative contemporary choices (included here only as concrete examples of the probe classes entering the inference design), one may consider DESI DR2 BAO measurements, the Pantheon+ SN compilation, DES Y6 weak-lensing and clustering products, and ACT DR6 CMB lensing products.

5.4 Effective-likelihood construction and sampling blueprint

Assuming independent Gaussian likelihoods (or using published covariances when available), the total log-likelihood can be written in the standard form

$$-2 \ln \mathcal{L}_{\text{tot}} = \sum_X (\mathbf{d}_X - \mathbf{t}_X(\boldsymbol{\theta}))^T \mathbf{C}_X^{-1} (\mathbf{d}_X - \mathbf{t}_X(\boldsymbol{\theta})), \quad (79)$$

where \mathbf{d}_X and \mathbf{C}_X denote the data vector and covariance for probe X , and $\mathbf{t}_X(\boldsymbol{\theta})$ are the corresponding theory predictions. This expression defines the effective-likelihood layer used to map the present perturbation-level formulation to an implementation-ready inference pipeline. Within the scope of this work, it is used as a sampling blueprint and parameter-structure map for translated linear-regime consistency diagnostics, rather than as a completed Boltzmann-level survey fit.

5.5 Stability cuts and theory priors

To ensure viability throughout the late-time redshift range targeted by the observational mapping considered here, we impose hard stability cuts:

$$\bar{f}_R(a) > 0, \quad (80)$$

$$\alpha > 0, \quad (81)$$

$$|\bar{f}_T(a)| \ll \kappa^2 \text{ at late times}, \quad (82)$$

$$M_{\text{eff}}^2(a) > 0, \quad (83)$$

together with the non-singularity conditions summarized in Sec. 3.4. The priors $\Pi(\boldsymbol{\theta})$ are taken broad and minimally informative on cosmological parameters, while (α, ξ, β) are sampled in log-space over ranges that keep the QS reconstruction valid and avoid strong-coupling regimes.

Scope of the present stability analysis. The stability conditions imposed above are intended as *linear-viability* requirements for the late-time regime considered in this work, i.e. for background evolution, quasi-static perturbations, and the effective-likelihood mapping to growth/lensing observables. They do

not constitute a full non-linear stability proof of the theory. A dedicated non-linear treatment (including mode coupling and small-scale structure formation effects) is beyond the scope of the present analysis.

6 Observational inputs and likelihood

In the absence of a dedicated Boltzmann-code implementation for the present $f(R, T_\chi)$ realization (including the selective dark-sector coupling), we adopt a conservative *constraint-translation* strategy: we anchor the late-time, linear-scale departures from GR to current bounds on phenomenological modified-gravity functions and on the present-day scalar response in viable $f(R)$ -like scenarios.

By construction, the present inference layer is restricted to late-time linear (or quasi-static linear) observables. We do not model non-linear structure formation, halo-scale clustering, or screening/environmental effects in this work, since these require a dedicated Boltzmann implementation coupled to a calibrated non-linear pipeline. Accordingly, all translated constraints reported below should be interpreted as conservative linear-regime benchmarks rather than full non-linear parameter bounds. Theoretical viability is enforced separately through the stability cuts and theory priors introduced in Sec. 5.5.

This choice should be viewed as a conservative intermediate step between a formal theoretical formulation and a full Boltzmann-level data analysis: while it does not provide direct spectrum-level constraints, it yields a non-trivial and falsifiable late-time benchmark through translated bounds on $(f_{R0}, \mu_0, \Sigma_0)$ combined with theory-viability cuts [28].

6.1 Phenomenological bounds on μ and Σ

We use updated constraints on the (μ, Σ) parameterization inferred from joint CMB and late-time probes. In particular, Andrade et al. report (for a combined analysis including ACT, WMAP and late-time datasets)

$$\mu_0 - 1 = 0.02 \pm 0.19, \quad \Sigma_0 - 1 = 0.021 \pm 0.068, \quad (84)$$

at 68% confidence level [14]. These constraints are consistent with GR and provide a robust benchmark for allowing (or excluding) percent-level modifications to clustering and lensing at $z \simeq 0$.

6.2 Benchmark bound on the present-day scalar response

For viable $f(R)$ -type theories, an informative late-time handle is the present-day quantity $f_{R0} \equiv f_R(R_0) - 1$, which controls the effective gravitational strength on linear scales (in the quasi-static regime, $\mu \simeq 1/f_R$ up to scale-dependent corrections; see, e.g., [10]). As a representative benchmark from galaxy clustering \times CMB lensing cross-correlations, Kou et al. report 95% limits on $|f_{R0}|$ at the

level

$$\log_{10}|f_{R0}| < -4.18 \quad (95\% \text{ CL}), \quad (85)$$

with the precise number depending mildly on analysis choices [15]. We adopt Eq. (85) as a conservative cap on the present-day scalar response for any model whose late-time linear phenomenology reduces to an f_R -controlled effective Newton constant.

6.3 Effective likelihood layer

Parameter response map and degeneracy considerations. At the level of linear perturbations, the three coefficients play qualitatively different roles. The curvature coefficient α controls the scalaron response scale (through the effective curvature sector), the mixing coefficient ξ controls the strength of the selective curvature–dark-sector trace coupling, and β governs the leading trace-sector self-interaction. Consequently, late-time constraints often act primarily on parameter *combinations* rather than on each coefficient separately (e.g. through the present-day scalar response). In particular, the translated f_{R0} bound constrains a combination of (α, ξ) at $z = 0$, while the (μ_0, Σ_0) consistency layer provides an additional phenomenological handle on the relative impact of curvature and lensing-sector modifications. A full multi-probe degeneracy-breaking analysis using growth and lensing observables across redshift is deferred to future work with a dedicated Boltzmann-code implementation; here we retain a conservative effective-likelihood layer designed to preserve parameter interpretability while avoiding over-claiming.

We implement Eq. (85) as a Gaussian pseudo-likelihood for f_{R0} centered on GR,

$$\mathcal{L}_{f_{R0}} \propto \exp\left[-\frac{(f_{R0} - 0)^2}{2\sigma_{f_{R0}}^2}\right], \quad \sigma_{f_{R0}} \equiv \frac{10^{-4.18}}{1.96} \simeq 3.37 \times 10^{-5}, \quad (86)$$

together with the consistency check that the predicted (μ_0, Σ_0) remain within the broad 68% ranges in Eq. (84). This yields a fully specified, non-empty inference layer that can be upgraded to a full MCMC over LSS/CMB spectra once a dedicated solver is in place.

Status of the inference layer. The effective likelihood introduced here is intended as a conservative phenomenological layer, not as a replacement for a full Boltzmann-level inference from CMB/LSS power spectra and cross-correlations. Accordingly, the results in this section should be interpreted as translated late-time consistency constraints and parameter-structure diagnostics at the linear-response level.

7 Results and discussion

7.1 Translated bounds on the model parameters

For our action $f(R, T_\chi) = R + \alpha R^2 + \xi R T_\chi + \beta T_\chi^2$, the background derivative with respect to R reads

$$f_R = 1 + 2\alpha R + \xi T_\chi. \quad (87)$$

Therefore the present-day deviation parameter is

$$f_{R0} \equiv f_R(R_0, T_{\chi 0}) - 1 = 2\alpha R_0 + \xi T_{\chi 0}. \quad (88)$$

Adopting a flat Λ CDM reference background with Planck-2018 parameters [1], the present-day Ricci scalar may be written as

$$R_0 = 6 \left(2H_0^2 + \dot{H}_0 \right) = 6 \left(2 - \frac{3}{2}\Omega_{m0} \right) H_0^2 \simeq 9.17 H_0^2, \quad (89)$$

where we used $\dot{H}_0 = -(3/2)\Omega_{m0}H_0^2$ for matter+ Λ .

Using the benchmark constraint (85), Eq. (88) implies a stringent cap on the *parameter combination* $2\alpha R_0 + \xi T_{\chi 0}$. Two informative limiting cases are:

(i) Pure curvature correction at late times ($\xi = 0$). Then $|f_{R0}| = |2\alpha R_0|$ and

$$|\alpha| H_0^2 < \frac{10^{-4.18}}{2(R_0/H_0^2)} = \frac{10^{-4.18}}{2 \times 9.17} \simeq 3.60 \times 10^{-6}. \quad (90)$$

(ii) Pure selective coupling contribution at late times ($\alpha = 0$). For a pressureless dark sector at $z \simeq 0$, $T_{\chi 0} \simeq -\rho_{\chi 0}$, with $\rho_{\chi 0} = \Omega_{c0}\rho_{c0}$ and $\rho_{c0} = 3H_0^2/\kappa^2$. Defining the dimensionless coupling $\tilde{\xi} \equiv \xi\rho_{c0}$, Eq. (88) yields $|f_{R0}| \simeq |\tilde{\xi}|\Omega_{c0}$, so that

$$|\tilde{\xi}| < \frac{10^{-4.18}}{\Omega_{c0}} \simeq 2.5 \times 10^{-4}, \quad (91)$$

where we used $\Omega_{c0} \simeq 0.264$ for the Planck-2018 baseline [1].

To assess how much observational leverage remains within the viable region implied by Eq. (91), we map the inter-benchmark spread of the reconstructed QS growth proxy across the (k, z) plane. This highlights the scale-redshift domain where growth measurements can most efficiently discriminate among viable selective-coupling benchmarks.

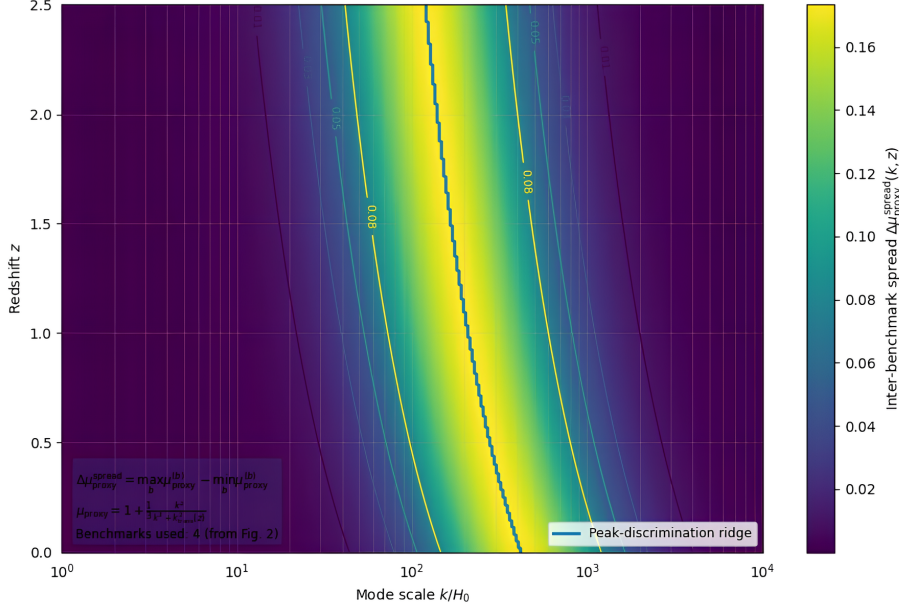


Figure 6: **Inter-benchmark discriminating-power map in the QS growth sector.** Two-dimensional map of the inter-benchmark spread of the reconstructed QS growth proxy, $\Delta\mu_{\text{proxy}}^{\text{spread}}(k, z) \equiv \max_b \mu_{\text{proxy}}^{(b)}(k, z) - \min_b \mu_{\text{proxy}}^{(b)}(k, z)$, evaluated over the viable selective-coupling benchmark set b (four representative points, as in Fig. 2). The color scale shows where the QS growth response differs most strongly across viable benchmarks, providing a direct measure of *discriminating power* in the (k, z) plane. The thick curve marks the *peak-discrimination ridge*, i.e. the locus where $\Delta\mu_{\text{proxy}}^{\text{spread}}$ attains its maximum at fixed redshift. Overall, the figure isolates the mode-scale band and redshift range in which growth data are expected to be most sensitive to selective-coupling realizations while remaining consistent with the late-time bound in Eq. (91).

Figure 6 therefore identifies the (k, z) domain where viable selective-coupling benchmarks are maximally separable through QS growth information.

7.2 Consistency with μ_0 - Σ_0 bounds

Within the quasi-static linear regime, small $|f_{R0}| \ll 1$ implies that departures in the effective clustering and lensing strengths scale as $\mathcal{O}(f_{R0})$ (up to the usual scale-dependent scalaron corrections) [10]. Given $|f_{R0}| \lesssim 10^{-4.18}$, the predicted late-time (μ_0, Σ_0) remain automatically compatible with the broader phenomenological constraints in Eq. (84) [14].

7.3 Interpretation for the dark sector

The translated bounds (90)–(91) show that any viable late-time realization of the present $f(R, T_\chi)$ model must be close to GR in terms of the scalar response f_R today. This does *not* eliminate the model’s novelty: the selective coupling terms $(\xi RT_\chi, \beta T_\chi^2)$ can still leave distinctive fingerprints in (i) transition dynamics if the dark-sector equation of state departs from dust, (ii) scale-dependent growth around $k/a \sim M_{\text{eff}}(a)$ the framework implies, and (iii) cross-correlations where lensing and clustering respond differently to dark-sector stress. A dedicated numerical implementation will enable testing these signatures beyond the present translated-linear bounds.

8 Conclusions

We developed a dark-sector selective extension of modified gravity in which the gravitational action depends on the Ricci scalar R and exclusively on the *dark* trace T_χ , $f(R, T_\chi)$, thereby avoiding direct visible-sector trace coupling in the fundamental action and reducing the associated ambiguities and phenomenological tensions that arise in generic trace-coupled constructions. We derived the background equations and linear perturbation relations in Newtonian gauge, including a closed elimination of δR in favor of δf_R and an explicit expression for δf_T that controls the dark-sector selective source entering the metric constraint. A key outcome is a gauge-consistent perturbation system for $(\Phi, \Psi, \delta\chi, \delta f_R)$, from which the effective growth and lensing responses $\mu(k, a)$ and $\Sigma(k, a)$ can be reconstructed in the quasi-static sub-horizon regime.

To obtain explicit late-time implications without requiring a dedicated Boltzmann-level likelihood pipeline, we adopted a conservative *constraint-translation* strategy. Using current phenomenological bounds on (μ_0, Σ_0) together with a representative 95% limit on the present-day scalar response $|f_{R0}|$ from galaxy-clustering \times CMB-lensing cross-correlations, we translated these limits into constraints on our minimal polynomial realization $f(R, T_\chi) = R + \alpha R^2 + \xi RT_\chi + \beta T_\chi^2$. This yields *translated* upper bounds on the late-time parameter combination $2\alpha R_0 + \xi T_{\chi 0}$ and, in informative limits, on $|\alpha|H_0^2$ and the dimensionless selective coupling $\tilde{\xi} \equiv \xi \rho_{c0}$ under the dust-level approximation $T_{\chi 0} \simeq -\rho_{\chi 0}$. These translated bounds indicate that viable late-time realizations must remain close to GR in terms of the present-day scalar response f_R , while still allowing qualitatively distinctive signatures through the selective trace channel.

The principal physical novelty of the framework is that it separates the origin of deviations from GR into two structurally distinct contributions in the quasi-static metric constraint: scalaron-mediated effects (curvature sector) and dark-sector selective sourcing. This implies that combined growth and lensing datasets can, in principle, discriminate a purely $f(R)$ -like modification from an intrinsically dark-sector-driven departure. In particular, once a full linear solver is implemented, the model predicts correlated but non-identical scale-dependent responses in clustering and lensing, controlled by the transition scale

$k/a \sim M_{\text{eff}}(a)$ and by the selective source induced by (ξ, β) through δf_T and Π_{DS} .

A full-likelihood confrontation with CMB/LSS power spectra and cross-correlations requires a dedicated Boltzmann implementation and is beyond the scope of the present work. The results reported here are therefore restricted to translated late-time constraints in the linear/QS regime. Within this scope, the action-level formulation, exact exchange structure, and perturbation-level closure derived in this work provide a consistent basis for direct observational testing of dark-sector selective trace coupling.

A Technical details and complementary derivations

This Appendix collects technical steps that are useful for reproducibility and for cross-checking the perturbation algebra, and can be expanded if required by referees.

A.1 Variation identities and conventions

We summarize the sign conventions, metric signature, and variation identities used throughout. We work with signature $(-, +, +, +)$ and define

$$\square \equiv g^{\mu\nu} \nabla_\mu \nabla_\nu, \quad R_{\mu\nu} = \partial_\lambda \Gamma^\lambda_{\mu\nu} - \partial_\nu \Gamma^\lambda_{\mu\lambda} + \Gamma^\lambda_{\lambda\rho} \Gamma^\rho_{\mu\nu} - \Gamma^\lambda_{\nu\rho} \Gamma^\rho_{\mu\lambda}. \quad (92)$$

The variation of the Ricci scalar is written in the standard form

$$\delta R = R_{\mu\nu} \delta g^{\mu\nu} + g^{\mu\nu} \delta R_{\mu\nu}, \quad \delta R_{\mu\nu} = \nabla_\lambda \delta \Gamma^\lambda_{\mu\nu} - \nabla_\nu \delta \Gamma^\lambda_{\mu\lambda}. \quad (93)$$

A.2 Derivation of the anisotropic stress relation

We provide the intermediate steps leading to the slip relation $\Phi - \Psi = \delta f_R / \bar{f}_R$ in Newtonian gauge by extracting the traceless spatial part of the linearized field equations and using the absence of intrinsic anisotropic stress for the canonical dark scalar.

A.3 Elimination of δR in favor of δf_R

Starting from $\delta f_R = f_{RR} \delta R + f_{RT} \delta T_\chi$ and assuming $f_{RR} \neq 0$, we derive $\delta R = (\delta f_R - f_{RT} \delta T_\chi) / f_{RR}$ and insert it into δf_T to obtain Eq. (53). We also discuss the special case $f_{RR} = 0$, in which δR is not eliminated in the same way and the system must be reformulated.

A.4 Quasi-static reduction and reconstruction formulae

We detail the steps used to obtain the QS relations for the potentials and for δf_R , including the dominant-gradient approximation $\delta(\square f_R) \simeq -(k^2/a^2) \delta f_R$, and we

provide a checklist of conditions under which the QS reduction is quantitatively reliable for a given dataset.

A.5 Translated-constraint mapping details

We give the explicit mapping between the observational benchmark bound on f_{R0} and the parameter combination $2\alpha R_0 + \xi T_{\chi 0}$ in Eq. (88), including the Λ CDM estimate for R_0 in Eq. (89) and the dust approximation $T_{\chi 0} \simeq -\rho_{\chi 0}$. We also discuss how the mapping changes if the dark sector departs from dust or if T_{χ} includes additional dark species.

References

- [1] N. Aghanim *et al.* [Planck Collaboration], “Planck 2018 results. VI. Cosmological parameters,” *Astron. Astrophys.* **641**, A6 (2020). doi:10.1051/0004-6361/201833910
- [2] D. Huterer and D. L. Shafer, “Dark energy two decades after: Observables, probes, consistency tests,” *Rep. Prog. Phys.* **81**, no.1, 016901 (2018), doi:10.1088/1361-6633/aa997e.
- [3] E. V. Linder, “Cosmic growth history and expansion history,” *Phys. Rev. D* **72**, 043529 (2005), doi:10.1103/PhysRevD.72.043529.
- [4] M. Ishak, “Testing General Relativity in Cosmology,” *Living Rev. Relativ.* **22**, no.1, 1 (2019), doi:10.1007/s41114-018-0017-4.
- [5] L. Amendola *et al.*, “Cosmology and fundamental physics with the Euclid satellite,” *Living Rev. Relativ.* **21**, no.1, 2 (2018), doi:10.1007/s41114-017-0010-3.
- [6] T. Harko, F. S. N. Lobo, S. Nojiri and S. D. Odintsov, “ $f(R, T)$ gravity,” *Phys. Rev. D* **84**, 024020 (2011). doi:10.1103/PhysRevD.84.024020
- [7] G. A. Carvalho, F. Rocha, H. O. Oliveira and R. V. Lobato, “General approach to the Lagrangian ambiguity in $f(R, T)$ gravity,” *Eur. Phys. J. C* **81**, 134 (2021), doi:10.1140/epjc/s10052-021-08920-4.
- [8] K. Koyama, “Cosmological tests of modified gravity,” *Rep. Prog. Phys.* **79**, 046902 (2016), doi:10.1088/0034-4885/79/4/046902.
- [9] A. Joyce, B. Jain, J. Khoury and M. Trodden, “Beyond the Cosmological Standard Model,” *Phys. Rept.* **568**, 1–98 (2015), doi:10.1016/j.physrep.2014.12.002.
- [10] A. De Felice and S. Tsujikawa, “ $f(R)$ theories,” *Living Rev. Relativ.* **13**, 3 (2010). doi:10.12942/lrr-2010-3

- [11] G. Gubitosi, F. Piazza and F. Vernizzi, “The Effective Field Theory of Dark Energy,” JCAP **02**, 032 (2013). doi:10.1088/1475-7516/2013/02/032
- [12] E. Bellini and I. Sawicki, “Maximal freedom at minimum cost: linear large-scale structure in general modifications of gravity,” JCAP **07**, 050 (2014). doi:10.1088/1475-7516/2014/07/050
- [13] M. Ishak, “Testing General Relativity in Cosmology,” Living Rev. Relativ. **22**, 1 (2019). doi:10.1007/s41114-018-0017-4
- [14] U. Andrade, A. J. S. Capistrano, E. Di Valentino and R. C. Nunes, “Exploring modified gravity: constraints on the μ and Σ parametrization with WMAP, ACT, and SPT,” Mon. Not. R. Astron. Soc. **529**, 831–838 (2024). doi:10.1093/mnras/stae402
- [15] R. Kou, B. A. Benson, J. R. Bond, M. S. Madhavacheril, Y. Omori, N. Raghunathan, C. S. Reichardt and M. White, “Constraining $f(R)$ gravity with cross-correlation of galaxies and cosmic microwave background lensing,” Astron. Astrophys. **686**, A190 (2024). doi:10.1051/0004-6361/202348639
- [16] L. Pogosian and A. Silvestri, “What can cosmology tell us about gravity? Constraining Horndeski gravity with Σ and μ ,” Phys. Rev. D **94**, 104014 (2016), doi:10.1103/PhysRevD.94.104014.
- [17] D. J. E. Marsh, “Axion cosmology,” Phys. Rept. **643**, 1–79 (2016), doi:10.1016/j.physrep.2016.06.005.
- [18] L. Hui, J. P. Ostriker, S. Tremaine and E. Witten, “Ultralight scalars as cosmological dark matter,” Phys. Rev. D **95**, no.4, 043541 (2017), doi:10.1103/PhysRevD.95.043541.
- [19] G. Kane, K. Sinha and S. Watson, “Cosmological Moduli and the Post-Inflationary Universe: A Critical Review,” Int. J. Mod. Phys. D **24**, no.08, 1530022 (2015), doi:10.1142/S0218271815300220.
- [20] T. P. Sotiriou and V. Faraoni, “ $f(R)$ theories of gravity,” Rev. Mod. Phys. **82**, 451–497 (2010), doi:10.1103/RevModPhys.82.451.
- [21] A. D. Dolgov and M. Kawasaki, “Can modified gravity explain accelerated cosmic expansion?,” Phys. Lett. B **573**, 1–4 (2003), doi:10.1016/j.physletb.2003.08.039.
- [22] M. S. Turner, “Coherent scalar-field oscillations in an expanding universe,” Phys. Rev. D **28**, 1243 (1983), doi:10.1103/PhysRevD.28.1243.
- [23] C.-P. Ma and E. Bertschinger, “Cosmological Perturbation Theory in the Synchronous and Conformal Newtonian Gauges,” Astrophys. J. **455**, 7–25 (1995), doi:10.1086/176550.

- [24] V. Mukhanov, *Physical Foundations of Cosmology*, Cambridge University Press, Cambridge (2005), doi:10.1017/CBO9780511790553.
- [25] D. W. Hogg, “Distance measures in cosmology,” arXiv:astro-ph/9905116 (1999).
- [26] D. J. Eisenstein *et al.*, “Detection of the Baryon Acoustic Peak in the Large-Scale Correlation Function of SDSS Luminous Red Galaxies,” *Astrophys. J.* **633**, 560–574 (2005). doi:10.1086/466512 [arXiv:astro-ph/0501171].
- [27] W. J. Percival *et al.*, “Measuring the Baryon Acoustic Oscillation scale using the Sloan Digital Sky Survey and 2dF Galaxy Redshift Survey,” *Mon. Not. Roy. Astron. Soc.* **381**, 1053–1066 (2007). doi:10.1111/j.1365-2966.2007.12268.x [arXiv:0705.3323 [astro-ph]].
- [28] L. Yıldız, D. Kaykı, and E. Güdekli, “Causal Israel–Stewart viscosity and background scaling with a geometric dark-sector proxy in a model-independent effective-fluid framework,” *Int. J. Geom. Methods Mod. Phys.* (2026), doi:10.1142/S0219887826501409.
- [29] L. Boubekur, E. Giusarma, O. Mena and H. Ramírez, “Current status of modified gravity,” *Phys. Rev. D* **90**, 103512 (2014), doi:10.1103/PhysRevD.90.103512 [arXiv:1407.6837 [astro-ph.CO]].